First measurement of proton's charge form factor at very low Q2 with initial state radiation

Mihovilovič, M.; Weber, A. B.; Achenbach, P.; Beranek, T.; Beričič, J.; Bernauer, J. C.; Boehm, R.; Bosnar, Damir; Cardinali, M.; Correa, L.; ...

Source / Izvornik: **Physics Letters B, 2017, 771, 194 - 198**

Journal article, Published version
Rad u časopisu, Objavljena verzija rada (izdavačev PDF)

https://doi.org/10.1016/j.physletb.2017.05.031

Permanent link / Trajna poveznica: https://urn.nsk.hr/urn:nbn:hr:217:717867

Physics Letters B 771 (2017) 194–198

Contents lists available at ScienceDirect

Physics Letters B

www.elsevier.com/locate/physletb

First measurement of proton's charge form factor at very low Q^2 with initial state radiation

M. Mihovilovič [a,b], A.B. Weber [a], P. Achenbach [a], T. Beranek [a], J. Beričič [b], J.C. Bernauer [c], R. Böhm [a], D. Bosnar [d], M. Cardinali [a], L. Correa [e], L. Debenjak [b], A. Denig [a], M.O. Distler [a], A. Esser [a], M.I. Ferretti Bondy [a], H. Fonvieille [e], J.M. Friedrich [f], I. Friščić [d], K. Griffioen [g], M. Hoek [a], S. Kegel [a], Y. Kohl [a], H. Merkel [a,*], D.G. Middleton [a], U. Müller [a], L. Nungesser [a], J. Pochodzalla [a], M. Rohrbeck [a], S. Sánchez Majos [a], B.S. Schlimme [a], M. Schoth [a], F. Schulz [a], C. Sfienti [a], S. Širca [h,b], S. Štajner [b], M. Thiel [a], A. Tyukin [a], M. Vanderhaeghen [a], M. Weinriefer [a]

[a] Institut für Kernphysik, Johannes Gutenberg-Universität Mainz, DE-55128 Mainz, Germany
[b] Jožef Stefan Institute, SI-1000 Ljubljana, Slovenia
[c] Massachusetts Institute of Technology, Cambridge, MA 02139, USA
[d] Department of Physics, University of Zagreb, HR-10002 Zagreb, Croatia
[e] Université Clermont Auvergne, CNRS/IN2P3, LPC, BP 10448, F-63000 Clermont-Ferrand, France
[f] Technische Universität München, Physik Department, 85748 Garching, Germany
[g] College of William and Mary, Williamsburg, VA 23187, USA
[h] Faculty of Mathematics and Physics, University of Ljubljana, SI-1000 Ljubljana, Slovenia

ARTICLE INFO

Article history:
Received 30 March 2017
Accepted 11 May 2017
Available online 15 May 2017
Editor: V. Metag

Keywords:
Initial state radiation
Proton
Form factor
Radiative corrections

ABSTRACT

We report on a new experimental method based on initial-state radiation (ISR) in e–p scattering, which exploits the radiative tail of the elastic peak to study the properties of electromagnetic processes and to extract the proton charge form factor (G_E^p) at extremely small Q^2. The ISR technique was implemented in an experiment at the three-spectrometer facility of the Mainz Microtron (MAMI). This led to a precise validation of radiative corrections far away from elastic line and provided first measurements of G_E^p for $0.001 \leq Q^2 \leq 0.004\,(\mathrm{GeV}/c)^2$.

1. Introduction

The radius of the proton as a fundamental subatomic constant has recently received immense attention. The CODATA [1] value of 0.8751(61) fm was compiled from electron scattering and atomic Lamb shift measurements. Both approaches gave consistent results. This value however, does not agree with the findings of very precise Lamb shift measurements in muonic hydrogen [2,3], which report a value of 0.84087(39) fm, which is a 6σ discrepancy with respect to the CODATA value. This discrepancy cannot be explained within existing physics theories, nor can it be interpreted as an experimental error. To provide further insight into the matter, several new spectroscopic and scattering experiments are underway. They aim to investigate different aspects of the problem [4–6].

In a scattering experiment the charge radius of the proton is typically determined by measuring cross sections for elastic scattering of electrons from hydrogen, which depend on G_E^p and carry information about the charge distribution in the proton. The proton charge radius is given by

$$r_p^2 \equiv -6\hbar^2 \left.\frac{\mathrm{d}G_E^p}{\mathrm{d}Q^2}\right|_{Q^2=0}, \tag{1}$$

where Q^2 is the negative square of the four-momentum transferred to the hadron. Due to the limited reach of existing data sets ($Q^2 > 0.004\,\mathrm{GeV}^2/c^2$) the slope of G_E^p at $Q^2 = 0$ needs to be evaluated from an extrapolated fit of the measured data. The

* Corresponding author.
E-mail address: merkel@kph.uni-mainz.de (H. Merkel).

http://dx.doi.org/10.1016/j.physletb.2017.05.031

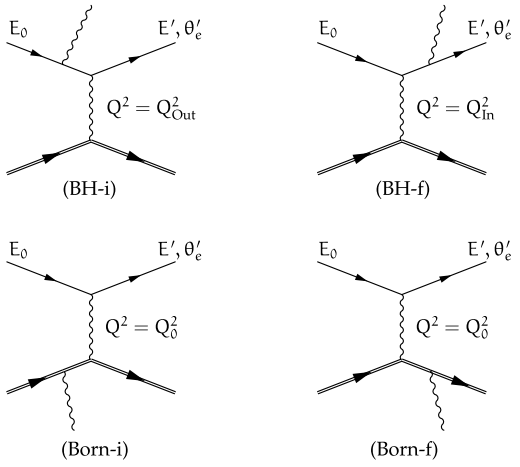

Fig. 1. Feynman diagrams for inelastic scattering of an electron from a proton, where an electron or a proton emits a real photon before or after the interaction. Diagrams where electrons emit a photon are known as Bethe–Heitler (BH) diagrams, while those where protons emit real photons are called Born diagrams. Q^2_{In} is the squared four-momentum fixed by the beam energy and the scattering angle, while $Q^2_{\text{Out}} \leq Q^2_{\text{In}}$ corresponds to the value measured with the detector. $Q^2_0 = 4E_0E'\sin^2(\theta'_e/2)/c^2$, where E_0 is the energy of the incident electron, E' and θ'_e are the energy and angle of the detected electron. For the (BH-i) diagram $Q^2 = Q^2_{\text{Out}}$, and for the (BH-f) diagram $Q^2 = Q^2_{\text{In}}$.

available data have enough resolving power to precisely determine the slope of the form factor at some distance from the origin, but additional data are needed to constrain the slope at $Q^2 = 0$. Therefore, measurements of G_E^p need to be extended into the previously unmeasured region of $Q^2 \lesssim 10^{-3}\,\text{GeV}^2/c^2$.

Efforts to do such measurements with the standard approaches are limited by the minimal Q^2 accessible with the experimental apparatus at hand. The energy of the electron beam and the scattering angle must be very small. Here we present a new experimental approach that avoids these kinematic limitations, extends the currently accessible Q^2 range, and allows for a precise test of radiative corrections, which impact the extractions of form factor from elastic scattering experiments, and for cross section measurements below $0.004\,\text{GeV}^2/c^2$ with sub-percent precision. The initial state radiation (ISR) technique exploits information within the radiative tail of the elastic peak. This was inspired by a similar concept used in particle physics to measure $e^+e^- \to$ hadrons over a wide range of center-of-mass energies in a single experiment [7,8].

2. Initial state radiation technique

The radiative tail of an elastic peak is dominated by the contributions from two Bethe–Heitler diagrams [9] as shown in Fig. 1. The initial-state radiation (BH-i) corresponds to the incident electron emitting a real photon before interacting with the proton, and the final-state radiation (BH-f) corresponds to a real photon being emitted after the interaction with the nucleon. For these processes two characteristic Q^2 can be defined:

$$Q^2_{\text{In}} = \frac{4\frac{E_0^2}{c^2}\sin^2\frac{\theta'_e}{2}}{1+\frac{2E_0}{Mc^2}\sin^2\frac{\theta'_e}{2}} \quad \text{and} \quad Q^2_{\text{Out}} = \frac{4\frac{E'^2}{c^2}\sin^2\frac{\theta'_e}{2}}{1-\frac{2E'}{Mc^2}\sin^2\frac{\theta'_e}{2}}.$$

Here, Q^2_{In} represents the value set by the chosen kinematics for elastic scattering (E_0, θ'_e), while Q^2_{Out} corresponds to the value measured by the detectors after scattering. E_0 and E' are the energies of the incoming and scattered electrons, M is the mass of the proton, and θ'_e is the scattering angle of the detected electron. In the limit of exact elastic $\text{H}(e,e')p$ scattering, Q^2_{In} and Q^2_{Out} are both equal to $Q^2_0 = 4E_0E'\sin^2(\theta'_e/2)/c^2$ and correspond to the Q^2 actually transferred to the proton. In $\text{H}(e,e')\gamma p$, however, Q^2_{In} and Q^2_{Out} no longer coincide. In the initial-state radiation diagram the emitted photon carries away part of the incident electron's four-momentum and opens the possibility to probe the proton's electromagnetic structure at $Q^2 = Q^2_{\text{Out}}$ which is smaller than Q^2_{In}. On the other hand, in the final-state radiation diagram the momentum transfer at the vertex remains fixed ($Q^2 = Q^2_{\text{In}}$), thus only Q^2_{Out} is modified, $Q^2_{\text{Out}} \leq Q^2$.

In an inclusive (e,e') experiment only Q^2_{Out} can be measured, which implies that initial state radiation cannot be distinguished from final state radiation. The measured radiative tail represents an approximately 2 : 3 mixture of terms with $Q^2 = Q^2_{\text{In}}$ and $Q^2 = Q^2_{\text{Out}}$, respectively. The Born terms (Born-i and Born-f), where the initial and final protons emit real photons, are suppressed by the mass of the proton but still have to be included as well as higher-order radiative corrections that also contribute to the radiative tail. The basic concept of the ISR approach is to isolate the interesting (BH-i) process from other contributions to the radiative tail, and thus obtain information on form factors at unmeasured values of $Q^2 = Q^2_{\text{Out}}$. To accomplish this, the measurements need to be studied in conjunction with a Monte-Carlo simulation that encompasses a comprehensive description of the radiative tail.

3. Description of the radiative tail

To realistically mimic the radiative tail, the peaking approximation models devised from the corrections to the elastic cross section are insufficient [9]. For an adequate description far away from the elastic line ($Q^2 = Q^2_{\text{Out}} \ll Q^2_{\text{In}}$), it is crucial to consider cross-section contributions to the e^8-order. To achieve this goal, a Monte-Carlo simulation is used, which employs a sophisticated event generator that exactly calculates the coherent sum of the amplitudes for the leading (e^3-order) diagrams shown in Fig. 1, and includes G_E^p as a free, tuneable parameter for every simulated Q^2. The next order vacuum polarization diagrams (with electrons inside the fermion loop) are exactly calculable and are added as a multiplicative factor to the cross section. The virtual corrections to the Bethe–Heitler diagrams (self-energy corrections and various vertex corrections) require integration of the loop diagrams and are computationally too intensive to be added directly to the simulation. Instead they are considered as effective corrections to the cross section using the prescription of Ref. [9], together with the real second-order correction (emission of two real photons) which is approximated using the corrections to the elastic cross section [9,10]. Hadronic corrections are also considered in the elastic limit using the calculations of Ref. [10]. They contribute only up to 0.5% to the cross section at the lowest energy settings. In the simulation the proton is always on-shell. Effects related to the internal structure of the proton, described by the general polarisabilities [11] and known from the virtual Compton scattering (VCS) experiments [12], were small and could be neglected. Besides the internal corrections, the simulation includes external radiative and Coulomb corrections [13,14], collisional losses of particles on their way from the vertex point to the detectors, and the precise acceptances of the spectrometers.

4. Experiment

The measurement of the radiative tail has been performed at the Mainz Microtron (MAMI) in 2013 using the spectrometer setup of the A1-Collaboration [15]. In the experiment a rastered electron beam with energies of 195, 330 and 495 MeV was used in combination with a hydrogen target, which consisted of a 5 cm-long

cigar-shaped Havar cell filled with liquid hydrogen and placed in an evacuated scattering chamber. For the cross section measurements the single-dipole magnetic spectrometer B was employed. It was positioned at a fixed angle of 15.21°, while its momentum settings were adjusted to scan the complete radiative tail for each beam energy. The central momentum of each setting was measured with an NMR probe to a relative accuracy of 8×10^{-5}. The spectrometer is equipped with a detector package consisting of two layers of vertical drift chambers (VDCs) for tracking, two layers of scintillation detectors for triggering, and a threshold Cherenkov detector for particle identification. The kinematic settings of the experiment were chosen such that the radiative tails recorded at three beam energies overlap.

The beam current was between 10 nA and 1 μA and was limited by the maximum rate allowed in the VDCs (≈ 1 kHz/wire), resulting in raw rates up to 20 kHz. The current was determined by a non-invasive fluxgate-magnetometer and from the collected charge of the stopped beam. At low beam currents and low beam energies the accuracy of both approaches is not better than 2%, which is insufficient for a precision cross section measurement. Hence spectrometer A, used in a fixed momentum and angular setting, was employed for precise monitoring of the relative luminosity.

In spite of the good vacuum conditions inside the scattering chamber (10^{-6} mbar), the experiment was sensitive to traces of cryogenic depositions on the target walls, consisting mostly of residual nitrogen and oxygen present in the scattering chamber [16]. Since the deposited layer affected the measured spectra, the kinematic settings for spectrometer A were chosen such that the nitrogen/oxygen elastic lines were always visible next to the hydrogen spectrum, which served as a precise monitor of the thickness of the cryogenic depositions.

5. Data analysis

Measurements at the highest beam energy settings encompass the range of Q^2 where G_E^p is known from previous experiments, and were then used for the validation of the ISR technique. The measurements with the beam energies of 330 MeV and 195 MeV were used to investigate G_E^p at previously unattained values of Q^2.

Before comparing the data to the simulation, the measured spectra had to be corrected for the inefficiencies of the detection system. The efficiencies of the scintillation detector and the Cherenkov detector were determined to be $(99.8 \pm 0.2)\%$ and $(99.74 \pm 0.02)\%$, respectively, and were considered as multiplicative correction factors to the measured distributions. The quality of the agreement between the data and simulation depends also on the momentum and spatial resolutions of the spectrometer. These were determined from dedicated calibration data sets. The relative momentum plus angular and vertex resolutions (FWHM) were 1.7×10^{-4}, 3 msr, and 1.6 mm, respectively.

A series of cuts were applied to the data in order to minimize the background. First, a cut on the Cherenkov signal was applied to identify electrons, followed by a cut on the nominal momentum acceptance of the spectrometer. To minimize the contributions of events coming from the target walls and cryogenic depositions, a rather strict, ±10 mm cut on the vertex position was applied. Due to the finite vertex resolution some of the background events remained in the cut sample. Their contribution to the spectra was estimated by using a dedicated simulation, normalized to the size of the nitrogen, oxygen and Havar elastic lines, and corrected for the changes in the thickness of the depositions versus time by using the data of Spectrometer A.

The most challenging background came from the entrance flange of spectrometer B and the metal support structure of the target cell. When measuring far away from the elastic peak, the elastically scattered electrons, which a priori are not accepted, undergo secondary processes in these components and re-scatter into the acceptance of the spectrometer. At high E' these contributions are negligible, but at low E', where the cross section for the Bethe–Heitler processes becomes comparable to the probability for double scattering, these secondary reactions begin to contribute substantially to the detected number of events. At high beam energy settings, the background can be successfully removed via strict cuts on vertex and out-of-plane angle. However, at the lowest energy settings, a substantial part remained inside the data, which limited our efforts to measure at lower Q^2. Since this background could not be adequately subtracted or simulated, the data with $E' < 128$ MeV were omitted from the present analysis, which limited the reach of the experiment to $Q^2 \geq 1.3 \cdot 10^{-3}\,\mathrm{GeV}^2/c^2$.

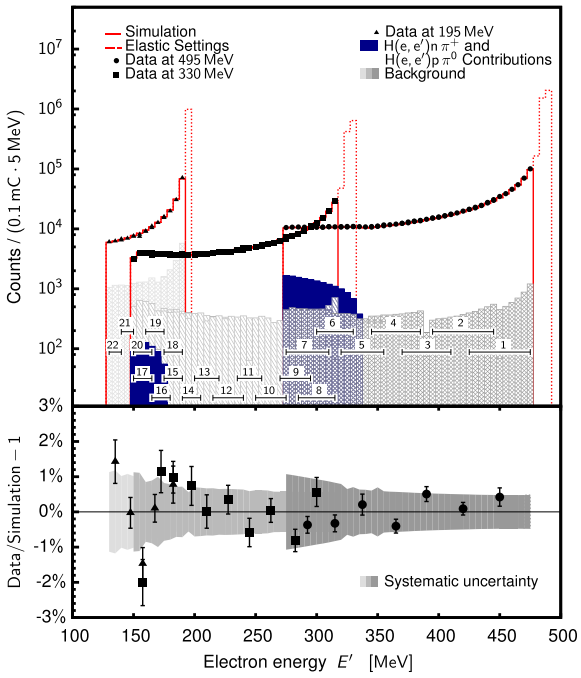

Fig. 2. (Color online.) Comparison of the data to the simulation. **Top:** Circles, squares and triangles show the measured distributions at 495 MeV, 330 MeV and 195 MeV, respectively, normalized to the accumulated charge of 0.1 mC. The elastic data (dashed line) are omitted from the analysis. The simulations with G_E^p, given by parameterization of Bernauer [17] are shown with red lines. The measurements at 495 MeV, 330 MeV, 195 MeV were divided into seven $(1-7)$, ten $(8-17)$ and five $(18-22)$ energy bins, respectively, such that two neighboring settings overlap for a half of the energy acceptance. The residual contributions of target walls, target frame, spectrometer entrance flange and cryogenic depositions are shown with shaded areas. The full (blue) areas represent the contributions of the pion production processes. **Bottom:** Relative difference between the data and simulation. The points show the mean values for each kinematic point, while the error bars denote their statistical uncertainties. Gray bands demonstrate the systematic uncertainties.

Additionally, the external corrections in the target material are not considered to the same order of precision as the internal radiative corrections. This is not problematic in the region of the tail, where the size of the former is small. However, in the immediate vicinity of the elastic peak, where their contribution is substantial, they may result in an incorrect description of the momentum distribution. To avoid this problem, the unradiated elastic data (from the first bin) were omitted from the analysis.

The cleaned event samples for each kinematic setting were corrected for the dead-time and prescale factors, weighted by the relative luminosity determined by spectrometer A, and then merged together to form a single spectrum that could be compared to the simulation (see Fig. 2). The simulation was performed with the Bernauer parameterization of G_E^p [17]. The contribution of G_M^p to

the cross section at $Q^2 \leq 10^{-2}\,\mathrm{GeV}^2/c^2$ is smaller than 0.5% and can therefore be approximated with the standard dipole model. For each beam-energy setting golden data were selected which served as a reference for the relative normalization of luminosity for other data sets. Hence, for each of the three beam energies one parameter (absolute luminosity) remained unknown and was fixed by equating the average ratio of data to simulation to unity.

In the bins far away from the elastic peak, one also needs to consider $\mathrm{H}(e,e')n\pi^+$ and $\mathrm{H}(e,e')p\pi^0$ reactions, which contribute up to 10% of all events. These processes were simulated using the MAID model [18] and were added to the full simulation before comparing it to the data.

6. Systematic uncertainties

The ISR technique provides remarkable control over the systematic uncertainties. With the fixed angular settings and overlapping momentum ranges all ambiguities related to the acceptances disappear. Furthermore, the luminosity is directly measured with spectrometer A, thus avoiding potential problems with fluctuations in the beam current and target density. The relative luminosity is determined with an accuracy better than 0.17%. Other sources of systematic uncertainty are: the ambiguity in the determination of detector efficiencies (0.2%); the inconclusiveness of the background simulation at lowest momenta ($\leq 0.5\%$); the contribution of higher-order corrections, which are not included in the simulation (0.3%); and the contamination with events coming from the target support frame and the spectrometer entrance flange (0.4%). The bins containing pions are subjected to another 0.5% uncertainty of the MAID model near the pion production threshold. This contribution, which appears to be an important source of the systematic uncertainty, is significant only for the 495 MeV setting. For the measurements at 195 MeV and 330 MeV the contribution of pion production processes is less than 2% and the corresponding systematic uncertainty is $\leq 0.1\%$.

7. Results and outlook

The ratio of measured and calculated cross sections shown in Fig. 2 (bottom) are in agreement to within a percent for all three energies. Considering the Bernauer fit [17] as a credible description of G_E^p this demonstrates for the first time that the electromagnetic processes, which give rise to the radiative tail are understood to a few parts per thousand, even at 200 MeV below the elastic line. This is an important finding for the electron-induced experiments, such as VCS [19], which require precise knowledge of the radiative corrections.

The remaining inconsistencies between the data and simulation could be due to the higher-order effects that are missing in the simulation or unresolved backgrounds. However, they could also be attributed to the difference between the true values of G_E^p and the model used in the simulation. Hence, the results presented in Fig. 2 may also be considered in reverse. Assuming that the theoretical description of radiative corrections is flawless and that background processes are well under control, the differences between data and simulation have been used to extract new values of the proton charge form factor. We have determined G_E^p for $0.001 \leq Q^2 \leq 0.017\,\mathrm{GeV}^2/c^2$, thus significantly extending the low Q^2-range of available data. The new values shown in Fig. 3 are consistent with results of previous measurements [20–23] in the region of overlap. The extracted new G_E^p values were compared to the polynomial

$$G(Q^2) = 1 - \frac{r_p^2\,Q^2}{6\hbar^2} + \frac{a\,Q^4}{120\hbar^4} - \frac{b\,Q^6}{5040\hbar^6}\,, \qquad (2)$$

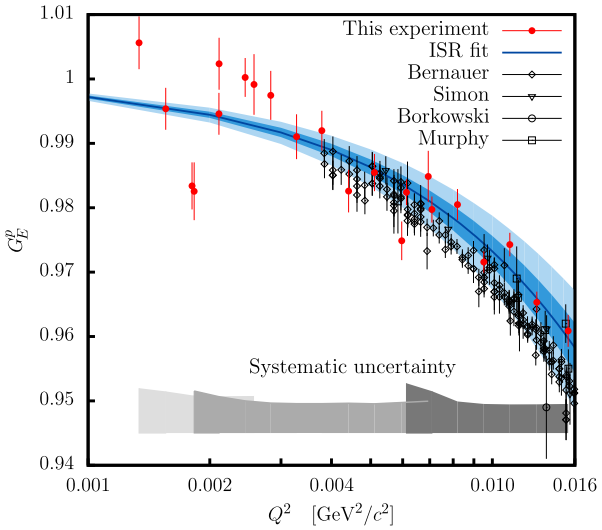

Fig. 3. (Color online.) The proton electric form factor as a function of $Q^2(=Q^2_{\mathrm{Out}})$. Empty black points show previous data [20–23]. The results of this experiment are shown with full red circles. The error bars show statistical uncertainties. Gray structures at the bottom shows the systematic uncertainties for the three energy settings. The curve corresponds to a polynomial fit to the data defined by Eq. (2). The inner and the outer bands around the fit show its uncertainties, caused by the statistical and systematic uncertainties of the data, respectively.

where parameters $a = (2.59 \pm 0.194)\,\mathrm{fm}^4$ and $b = (29.8 \pm 14.71)\,\mathrm{fm}^6$, which determine the curvature of the fit, were taken from Ref. [24]. The three data sets were fit with a common parameter for the radius, r_p, but with different renormalisation factors, n_{E_0}, for each energy. In terms of this fit with 18 degrees of freedom and χ^2 of 58.0, the normalisations and the radius were determined to be $n_{195} = 1.001 \pm 0.002_{\mathrm{stat}} \pm 0.003_{\mathrm{syst}}$, $n_{330} = 1.002 \pm 0.001_{\mathrm{stat}} \pm 0.003_{\mathrm{syst}}$, $n_{495} = 1.005 \pm 0.003_{\mathrm{stat}} \pm 0.007_{\mathrm{syst}}$, and $r_p = (0.810 \pm 0.035_{\mathrm{stat}} \pm 0.074_{\mathrm{syst}} \pm 0.003_{\Delta a,\Delta b})\,\mathrm{fm}$. The reduced χ^2 of 3.2 per degree of freedom (statistical uncertainties only) indicates that the results are dominated by systematic effects. Due to the limiting backgrounds and corresponding systematic uncertainties, we are unable to distinguish convincingly between the CODATA and the muonic hydrogen radii. However, we have proven the technique of initial state radiation to be a viable method for investigating the electromagnetic structure of the nucleon at extremely small Q^2. This has motivated further experiments of its kind. Utilising a gaseous point-like jet target together with a redesigned spectrometer entrance flange will significantly reduce instrumental backgrounds in the planned followup experiment [25] thereby extending G_E^p down to $Q^2 \approx 2 \cdot 10^{-4}\,\mathrm{GeV}^2/c^2$.

Acknowledgements

The authors would like to thank the MAMI accelerator group for the excellent beam quality which made this experiment possible. This work is supported by the Federal State of Rhineland-Palatinate, by the Deutsche Forschungsgemeinschaft with the Collaborative Research Center 1044, by the Slovenian Research Agency under Grant Z1-7305, by the Croatian Science Foundation under Project Number 1680 and U.S. Department of Energy under Award Number DE-FG02-96ER41003.

References

[1] P.J. Mohr, D.B. Newell, B.N. Taylor, Codata recommended values of the fundamental physical constants: 2014, Rev. Mod. Phys. 88 (2016) 035009, http://dx.doi.org/10.1103/RevModPhys.88.035009.

[2] R. Pohl, et al., The size of the proton, Nature 466 (7303) (2010) 213–216.

[3] A. Antognini, et al., Proton structure from the measurement of 2s–2p transition frequencies of muonic hydrogen, Science 339 (6118) (2013) 417–420, http://dx.doi.org/10.1126/science.1230016.
[4] R. Pohl, R. Gilman, G.A. Miller, K. Pachucki, Muonic hydrogen and the proton radius puzzle, Annu. Rev. Nucl. Part. Sci. 63 (2013) 175–204, http://dx.doi.org/10.1146/annurev-nucl-102212-170627.
[5] A. Gasparian, The PRad experiment and the proton radius puzzle, EPJ Web Conf. 73 (2014) 07006, http://dx.doi.org/10.1051/epjconf/20147307006.
[6] C.E. Carlson, The proton radius puzzle, Prog. Part. Nucl. Phys. 82 (2015) 59–77, http://dx.doi.org/10.1016/j.ppnp.2015.01.002.
[7] A.B. Arbuzov, E.A. Kuraev, N.P. Merenkov, L. Trentadue, Hadronic cross sections in electron–positron annihilation with tagged photon, J. High Energy Phys. 1998 (12) (1998) 009.
[8] B. Aubert, et al., J/ψ production via initial state radiation in $e^+e^- \to \mu^+\mu^-\gamma$ at an e^+e^- center-of-mass energy near 10.6 GeV, Phys. Rev. D 69 (2004) 011103, http://dx.doi.org/10.1103/PhysRevD.69.011103.
[9] M. Vanderhaeghen, J.M. Friedrich, D. Lhuillier, D. Marchand, L. Van Hoorebeke, J. Van de Wiele, QED radiative corrections to virtual Compton scattering, Phys. Rev. C 62 (2000) 025501, http://dx.doi.org/10.1103/PhysRevC.62.025501.
[10] L.C. Maximon, J.A. Tjon, Radiative corrections to electron–proton scattering, Phys. Rev. C 62 (2000) 054320, http://dx.doi.org/10.1103/PhysRevC.62.054320.
[11] H. Arenhövel, D. Drechsel, Generalized nuclear polarizabilities in $(e, e\gamma)$ coincidence experiments, Nucl. Phys. A 233 (1) (1974) 153–163, http://dx.doi.org/10.1016/0375-9474(74)90248-6.
[12] J. Roche, et al., First determination of generalized polarizabilities of the proton by a virtual Compton scattering experiment, Phys. Rev. Lett. 85 (2000) 708–711, http://dx.doi.org/10.1103/PhysRevLett.85.708.
[13] L.W. Mo, Y.S. Tsai, Radiative corrections to elastic and inelastic ep and up scattering, Rev. Mod. Phys. 41 (1969) 205–235, http://dx.doi.org/10.1103/RevModPhys.41.205.
[14] Y.-S. Tsai, Radiative corrections to electron–proton scattering, Phys. Rev. 122 (1961) 1898–1907, http://dx.doi.org/10.1103/PhysRev.122.1898.
[15] K. Blomqvist, et al., The three-spectrometer facility at the Mainz microtron MAMI, Nucl. Instrum. Methods Phys. Res., Sect. A 403 (2–3) (1998) 263–301, http://dx.doi.org/10.1016/S0168-9002(97)01133-9.
[16] M. Mihovilovič, et al., Initial state radiation experiment at MAMI, EPJ Web Conf. 72 (2014) 00017, http://dx.doi.org/10.1051/epjconf/20147200017.
[17] J.C. Bernauer, et al., Electric and magnetic form factors of the proton, Phys. Rev. C 90 (2014) 015206, http://dx.doi.org/10.1103/PhysRevC.90.015206.
[18] D. Drechsel, S. Kamalov, L. Tiator, Unitary isobar model – MAID2007, Eur. Phys. J. A 34 (1) (2007) 69–97, http://dx.doi.org/10.1140/epja/i2007-10490-6.
[19] P. Janssens, et al., A new measurement of the structure functions $P_{LL} - P_{TT}/\varepsilon$ and P_{LT} in virtual Compton scattering at $Q^2 = 0.33$ $(\mathrm{GeV}/c)^2$, Eur. Phys. J. A 37 (1) (2008) 1–8, http://dx.doi.org/10.1140/epja/i2008-10609-3.
[20] J.C. Bernauer, et al., High-precision determination of the electric and magnetic form factors of the proton, Phys. Rev. Lett. 105 (2010) 242001, http://dx.doi.org/10.1103/PhysRevLett.105.242001.
[21] G. Simon, C. Schmitt, F. Borkowski, V. Walther, Absolute electron–proton cross sections at low momentum transfer measured with a high pressure gas target system, Nucl. Phys. A 333 (3) (1980) 381–391, http://dx.doi.org/10.1016/0375-9474(80)90104-9.
[22] J.J. Murphy, Y.M. Shin, D.M. Skopik, Proton form factor from 0.15 to 0.79 fm^{-2}, Phys. Rev. C 9 (1974) 2125–2129, http://dx.doi.org/10.1103/PhysRevC.9.2125.
[23] F. Borkowski, P. Peuser, G. Simon, V. Walther, R. Wendling, Electromagnetic form factors of the proton at low four-momentum transfer, Nucl. Phys. A 222 (2) (1974) 269–275, http://dx.doi.org/10.1016/0375-9474(74)90392-3.
[24] M.O. Distler, J.C. Bernauer, T. Walcher, The RMS charge radius of the proton and Zemach moments, Phys. Lett. B 696 (4) (2011) 343–347, http://dx.doi.org/10.1016/j.physletb.2010.12.067.
[25] H. Merkel (spokesperson), The initial state radiation experiment with a jet target, MAMI proposal A1/02-16.